

# Computational Analysis of a Tip Vortex Structure Shed from a Bio-Inspired Blade

Sebastian Gomez<sup>1</sup>, Lindsay N. Gilkey<sup>2</sup>, Bryan E. Kaiser<sup>3</sup>, Svetlana V. Poroseva<sup>4</sup>  
*Department of Mechanical Engineering, University of New Mexico, Albuquerque, NM, 87131*

This study analyzes the effects that a bio-inspired blade shape has on the size and structure of a tip vortex. The blade prototype was selected based on the analysis of various insect orders with the purpose of finding wing profiles most suitable for the design of small rotorcraft propellers. Flow simulations are conducted around the bio-inspired blade and in its near wake using commercial CFD software Star-CCM+. Results are compared with those for a rectangular blade. A vortical structure is captured downstream of both blades. Flow data related to these structures is used to show that the bio-inspired shape produces weaker vortices, making it more desirable for rotorcraft implementation.

## Nomenclature

$c$	=	chord length
$C_L$	=	coefficient of lift
$C_D$	=	coefficient of drag
$IP$	=	figure of merit for desired characteristics
$f$	=	wing beat frequency
$k$	=	turbulent kinetic energy
$m$	=	insect mass
$r$	=	vortex radius
$r_c$	=	vortex core radius
$Re_c$	=	chord-based Reynolds number
$u_\theta$	=	tangential velocity
$u_{\theta max}$	=	maximum tangential velocity
$U$	=	insect flight velocity
$U_\infty$	=	freestream velocity
$U_D$	=	velocity deficit
$w$	=	axial component of velocity
$W$	=	wing loading

## I. Introduction

A vortex is recognized as an area in a fluid where a flow has a high level of rotation about an imaginary axis. Vortex phenomena are ever present in turbulent flows and are a mechanism for momentum transfer and energy dissipation. Mathematically, vortices are generated from the balance between the pressure gradient, the centrifugal force, and the Coriolis force in the momentum equation<sup>1</sup>. A specific type of vortex, called a tip vortex, is often encountered in lift-producing applications such as wings and blades. The pressure differential between the wing pressure and suction surfaces accelerates fluid around the wingtip, thus producing a tip vortex<sup>2</sup>.

---

<sup>1</sup> Graduate Student, Mechanical Engineering, 1 University of New Mexico MSC01 1150, Albuquerque, NM 87131, AIAA Student Member.

<sup>2</sup> Undergraduate Student, Mechanical Engineering, 1 University of New Mexico MSC01 1150, Albuquerque, NM 87131, AIAA Student Member.

<sup>3</sup> Graduate Student, Mechanical Engineering, 1 University of New Mexico MSC01 1150, Albuquerque, NM 87131, AIAA Student Member.

<sup>4</sup> Associate Professor, Mechanical Engineering, 1 University of New Mexico MSC01 1150, Albuquerque, NM 87131, AIAA Associate Fellow.

Tip vortices are characterized by high swirl velocities, low vortex core pressures, and axial velocity deficits with respect to the surrounding flow<sup>3</sup>. Tip vortices are undesirable because they reduce the wing lift and increase wing drag, which is also known as lift-induced drag<sup>2,4</sup>. Reduction of induced drag is highly sought after because close to 40% of the total drag on an aircraft is caused by this contribution to the total drag of a flying object<sup>2,5,6</sup>. Interactions between tip vortices and the fluid medium in which they exist may change the fluid properties substantially, leading to cavitation in hydrofoil applications<sup>2</sup>. Tip vortices are also a significant source of noise in helicopters and fixed-wing aircraft due to the highly unsteady flow in the vortices<sup>2,7</sup>. Based on the negative effects that tip vortices have on aircrafts and their surroundings, it can be concluded that the understanding and prediction of the tip vortex structure and vortex dynamics are of significant importance for all branches of aerodynamics.

Because wingtip geometry strongly affects vortex drag, wingtip optimization has received a great deal of attention<sup>5</sup>. As a result, a large number of patents for different mechanisms aiming to reduce tip vortices exist. The classical approach is to design wing geometry in such a way that it reduces tip vortices<sup>8-10</sup>. However, different methods such as active flow control by suction or blowing have been patented as well<sup>11-14</sup>. Difficulties related to the constant power supply necessary for active flow control make it unrealizable or highly inefficient for aircraft application; therefore, only geometric changes to wing profiles will be considered in this study. A number of studies have shown a decrease in tip vortex contribution to drag by making a variety of adjustments to wingtip geometry in aircraft. These adjustments include the addition of winglets, and endplates, and the modification of wingtip geometry<sup>4,6</sup>.

A substantial amount of research has also been done in flight of biological species. After all, nature is an excellent place to look for wing designs because flying creatures have evolved over millions of years to obtain efficient well-performing wings. Similar to aircraft wings, tip vortices play an important role in avian and insect flight despite of the vast differences in flight regimes of various species. The shape of bird wings has an impact on tip vortex behavior<sup>2</sup>. It has been determined that gliding birds, such as condors, use winglet-resembling features, called wing slots, at the tip of their wings to reduce induced drag<sup>16-17</sup>. Nature also seems to be aware of the effect that tip vortices have on acoustic noise production. It has been reported that owl wing tips are designed to minimize tip vortex noise to avoid being detected by prey<sup>2</sup>. Insect flight has proven to be much more difficult to understand than avian flight because measured forces in steady wind tunnel environments have been much smaller than required for insect flight<sup>18</sup>. To support the body weight, insect wings typically produce 2 to 3 times more lift than can be accounted for by conventional aerodynamics<sup>19</sup>. Insects are known for employing vortex formations to acquire the increased lift necessary for flight<sup>20</sup>. The tendency to stall at high angles of attack has been eliminated in insect flight by fluid interactions related to tip vortices<sup>21</sup>. Multiple studies have attributed high lift aerodynamics of insect flight to flow separation and vortex formation<sup>22</sup>. Many researchers have shown that wing corrugation improves lift via vortex generation<sup>23-26</sup>. An experimental study shows that the tip vortex contributes substantially to the lift produced by a flat plate with the aspect ratio and motion amplitudes similar to those found in Nature<sup>27</sup>. Based on the aforementioned findings, it seems like Nature has done a fantastic job producing realizable wing geometries that are capable of sustained flight in an efficient manner.

As it was previously mentioned, the flight regimes for birds and insects are very different. Applying Nature's strategies to fulfill engineering goals requires further definition of the engineering application so that the appropriate flight regime corresponding to specific biological species can be selected. The ultimate goal of our research is the design of a small flying vehicle suitable for a residential area. Currently, we are exploring a potential of vertical-take-off-landing (VTOL) vehicles such as small rotorcrafts for this purpose. Therefore, the objective of the current study is to select an insect that displays flight characteristics similar to those of small rotorcrafts. A rotor blade design based on the insect wing of choice is studied using computational fluid dynamics (CFD) tools. The magnitude and structure of the tip vortex generated by a bio-inspired blade is analyzed and its performance is compared with that of a rectangular blade.

## II. Insect Specie Selection

Advances in electronics and manufacturing methods have made small flying vehicles widely available to the public. It is assumed that with time, the size of such vehicles will grow, enabling personal rotorcrafts to be used for recreational and personal transportation purposes within and around city limits. Some of the desired rotorcraft characteristics include efficient propulsion mechanisms to reduce power consumption, low noise levels, a small foot print to enable vertical landings and take offs from locations with high obstacle density, the ability to achieve and sustain controlled flight and the option to carry a payload. Clearly, the geometry of the propeller(s) will play a crucial role on the performance, efficiency, and noise of a rotorcraft.

The ability to hover is an advantage of rotorcrafts. Since hovering is a seldom occurrence in avian flight, we chose to analyze insect species for our design goals. Interestingly enough, insects display many traits desirable in a VTOL vehicle: they fly efficiently to spend as little energy as possible, they produce low noise levels while in flight, they have been observed to fly in a wide range of flight conditions, their wing size is typically of the same order as their body, their flight is stable and controlled, and their shape and mass vary from order to order. In our study, we relied on data collected by biologists for different insect orders. The orders were categorized depending on their relative size, motion, and shape of the wings. From the existing insect orders, the following were considered<sup>28</sup> for the initial prescreening: Coleoptera (beetles), Heteroptera (true bugs), Blattaria (cockroaches), Lepidoptera (moths and butterflies), Odonta (dragonflies) Homoptera (aphids, cicadas and tree hoppers), Hymenoptera (ants, bees and wasps), Diptera (flies).

Insect orders containing multiple pairs of wings where the outer set is shell-like were dismissed because complicated aerodynamic interaction between both sets of wings would be extremely difficult to implement in a rotorcraft setting. The aforementioned restriction eliminated the Coleoptera, Heteroptera and Blattaria orders as options.

Insect orders possessing wings significantly larger than their body size, such as Lepidoptera (butterflies), were eliminated from consideration due to the VTOL vehicle requirement to have a small footprint. A rotorcraft blade generally has a small wing area compared to the largest body cross section, which eliminates the Odonta order because their wing areas are usually much larger than the largest body cross section. The wings of the remaining insect orders, Homoptera, Hymenoptera, and Diptera, needed to be subjected to further analysis through the use of data from biological studies to define the best candidate for the rotorcraft blade implementation.

Flight velocity, power consumption (in the form of wing beat frequency), payload carrying capabilities (in the form of insect mass), and a pre-existing metric, wing loading (ratio of mass to wing area), were used as variables to rate wings belonging to the remaining insect orders. Data for a number of insects considered during a previous study<sup>29</sup> is provided in Table 1.

**Table 1. Insect Parameters<sup>29</sup>**

Order	Species	Mass (g)	Wing Area (cm <sup>2</sup> )	Wing Loading (g/cm <sup>2</sup> )	Wingbeat Frequency (Hz)	Flight Velocity (m/s)	<i>IP</i> (g <sup>2</sup> /cm)
Diptera	Musca Domestica	0.012	0.200	0.060	190	1.97	7.5E-04
Hymenoptera	Apis sp.	0.021	0.200	0.105	130	2.55	4.3E-03
Hymenoptera	Euglossa Mandibularis	0.090	0.440	0.205	209	5.72	5.0E-02
Homoptera	Cicada sp.	0.752	7.640	0.098	42	2.21	3.9E-01

Using wing loading values as a measure to qualify desirable insect orders is not effective because all four insects have similar wing loading values despite of the variation in insect mass and wing area. Insects with small wings and large masses are still able to fly because their wing beat frequency is typically higher than that corresponding to an insect of the same mass with larger wing size<sup>30,31</sup>. However, increasing the wing beat frequency is not desirable for rotorcraft implementation because doing so would increase the acoustic noise, mechanical vibrations, and power consumption of the rotorcraft. Noting the limitation that wing beat frequency imposes on rotorcraft applications, it is a variable that should be taken into consideration when selecting an insect species. Wing beat frequency tends to be positively correlated with flight velocity and mass for most types of insects<sup>32</sup>. This creates a constraint on the approach to solely decrease wing beat frequency to improve the rotorcraft performance. A new challenge to minimize wing beat frequency without sacrificing flight velocity or weight-carrying capabilities (i.e.: insect mass) arises. A new figure of merit, *IP*, is introduced to quantify the desirable characteristics. *IP* is defined in a way that emphasizes the need to maximize weight-carrying capabilities and flight velocity while keeping wing beat frequency a minimum. *IP* is defined as

$$IP = \frac{mWU}{f} \quad (1)$$

where *m* is the insect mass, *W* is the wing loading value, *U* is the insect's maximum flight velocity, and *f* is the wing beat frequency. Calculated values of *IP* can be found in the last column of Table 1 for the corresponding insect species. Comparing values of *IP* from Table 1, one can notice that the *IP*-value corresponding to the cicada are at least an order of magnitude greater than for other insects.

After performing the qualitative analysis and a very basic quantification of insect characteristics included in this section, it has been concluded that cicadas are the best-suited candidates for rotorcraft applications. A beneficial byproduct of selecting cicadas is their relatively large size with respect to most insects. Larger wing characteristics should presumably scale better to larger scale applications, such as VTOL vehicles, and measurements of wing properties will be easier to perform. The main drawback of selecting an insect with a low wing beat frequency and a large size is that they tend to display less controlled flight behavior when compared to their counterparts. However, this drawback can be easily addressed without a substantial sacrifice in performance by employing well-tuned on-board control systems.

### III. Simulation Parameters

#### A. CAD Model

The insect wing used to generate the 3D CAD model was obtained from an adult cicada. The wing is composed of a brown venation structure, which provides structural integrity, and a very thin colorless obliterated membrane that acts as the lift-producing surface (Fig. 1). To generate the CAD model, measurements of the venation structure thickness were performed in the span-wise direction; however, the small size and large variations of vein features made it difficult to obtain accurate measurements throughout the entire wing. There was a slight amount of non-uniform camber present in the insect wing but it was not taken into account during the creation of the CAD model. A photograph of the wing sample was used to obtain an accurate representation of the overall wing shape. The wing outline in the photograph was used as a guide to draw the shape of the wing from the top perspective in the CAD package, SolidWorks. To ensure that the digital wing was dimensionally accurate, dimensioned lines were part of the photograph. The lengths of the dimensioned lines were matched accordingly in the SolidWorks environment. A wing thickness of 0.8 mm was used for both blades, which was a value in the range of recorded thickness measurements. The maximum length in the span direction of the model was 45.1 mm. Chord measurements ranged from 3.4 mm, near the base of the wing, to a maximum of 17.5 mm near the middle. The surface area of the resulting model was computed in SolidWorks as 576 mm<sup>2</sup>.

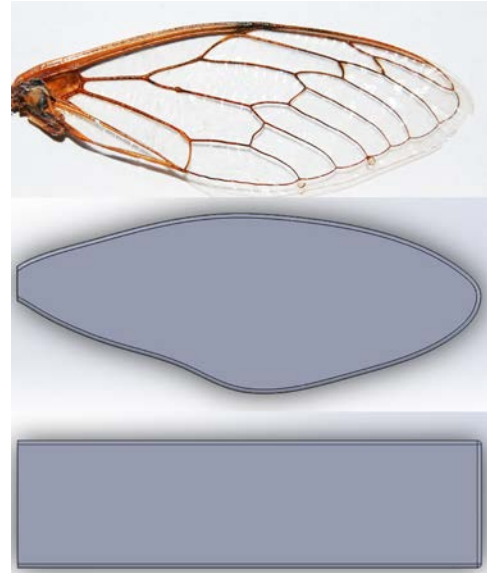


Figure 1. Cicada wing and CAD models

The procedure described above resulted in a blade with no camber or twist and with a uniform thickness. Square edges of the CAD model were rounded with a radius of 0.4 mm to facilitate meshing and reduce numerical instabilities in computations. The rectangular blade was designed to match the thickness, span length, and surface area of the bio-inspired wing, resulting in a chord length of 12.8 mm. Its edges were rounded similar to the bio-inspired blade. Figure 1 shows a side-by-side comparison of the cicada wing and the CAD models.

For the rotating blade simulations, the CAD models were scaled so the maximum chord length was 12.39 cm. The blades were fixed onto a hub that composed of a cylinder with the diameter of 2 chords and the length of 3 chords. Two hemispheres with a radius of 1 chord capped each side of the cylinder. The blades were fixed at location 1.25 chords along the hub.

#### B. Computational Domain

Different computational domains were used in flow simulations for fixed and rotating blades.

In the fixed blade simulations, dimensions of the computational volume are 0.25×0.3×0.4 m in the  $x$ -,  $y$ -, and  $z$ -directions, respectively. The origin is located at the bottom left corner of the computational domain (Fig. 2a). Figure 2a can be used to understand the orientation of the blade (shown in blue) with respect to the computational domain. The flow and blade chords are in the  $z$ -direction. The  $y$ -axis is normal to the flow direction and the blade spans are parallel to the  $x$ -axis. Within the computational domain, the blade is located in such a manner that its root is on the  $y$ - $z$  boundary of the domain corresponding to  $x=0$  m. The root chord line is located at  $y=0.15$  m, which places the blade in the middle of the computational domain in the  $y$ -direction. The midpoint of the root chord line is at  $x=0.175$  m from the inlet, which is equivalent to roughly 14 rectangular blade chord lengths.

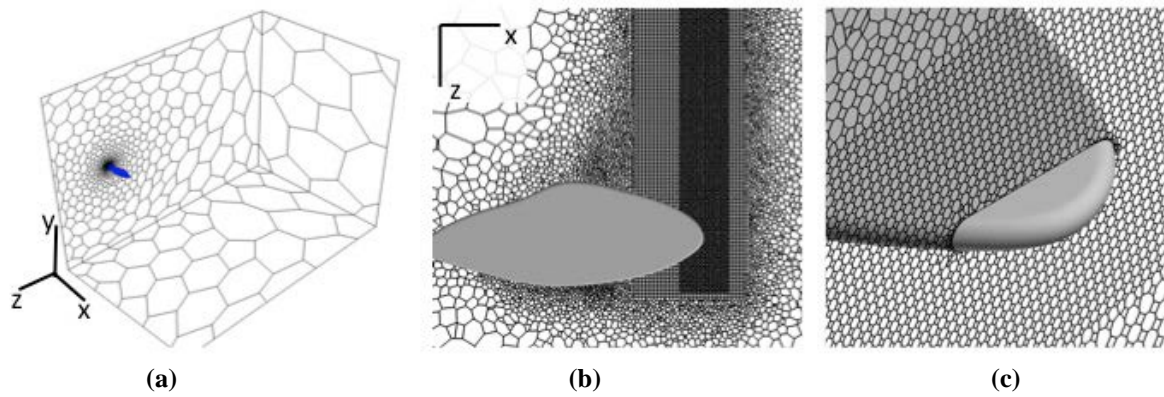


**Figure 2. Fixed blade: a) computational domain, b) volumetric controls, c) detailed view of the blade tip.**

The unstructured meshes were generated with Star-CCM+'s built-in mesh generator<sup>39</sup> using the Polyhedral Mesher, Surface Remesher, and Surface Wrapper models. A number of polyhedral mesh elements was varied from 0.5 million to 3 million. Two volumetric controls with elements of uniform size were incorporated into the meshes to detect the tip vortex and better resolve its structure. The volumetric controls are shown as lighter and darker rectangular areas in Figs. 2b and 2c. The absolute element size of the volumetric control section shown as the lighter rectangular area in Fig. 2b is  $6.5 \times 10^{-4}$  m. In the darker rectangle area, the absolute element size is  $4 \times 10^{-4}$  m. Outside of the volumetric controls, the minimum and target surface sizes are  $4 \times 10^{-4}$  m, and 1 m, respectively, and the surface growth rate is 1.3.

In the rotating blade simulations, the computational domain is measured in chord lengths of the rotating blades. The maximum chord length for the rotating blade simulations is 12.39 cm, and the dimensions of the computational volume are  $25 \times 25 \times 35$  chords in the  $x$ -,  $y$ -, and  $z$ - directions. The blades are placed at 10.25 chord lengths from the inlet in the  $z$ -direction. The blade hub is aligned in the  $z$ -direction. Figure 3a shows the rotating blade's orientation and location within the domain. A cylindrical region was created within the control volume that contained the blade and hub and rotated about the  $z$ -direction at the rate of 6 rps.

The number of elements used range from 611,000 to 3,179,000. Volumetric controls are used to control the cell size and density in the areas of interest, such as near the blade tips, along the path the tip vortices would travel in the wake, and the rotating region of the computational domain. The growth rate from the surfaces is 1.2. Outside the volumetric controls, the computational domain is filled with polyhedral cells. The growth rate of the polyhedral cells is 1.0 to ensure a high enough grid resolution in the wake area. Five prism layers were used around the blade and hub with a growth rate of 1.3 and a thickness of 0.05 chord lengths. Figure 3 shows the grid configuration at various locations.

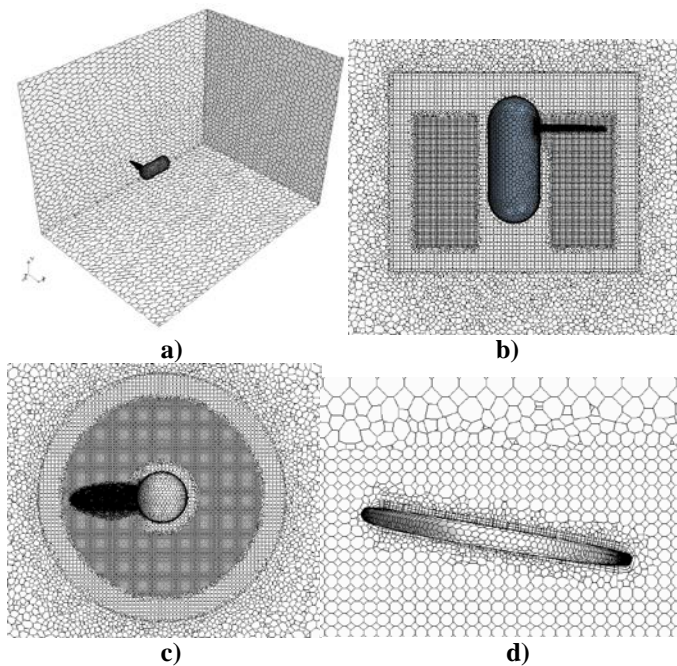


**Figure 3. Computational domains for rotating blades: a) computational volume, b) grid near rotating blades at  $y = 0$ , c) grid at blade looking down the axis of rotation at  $z = -10.25$  chords, d) grid at the location of max chord length.**

### C. Boundary Conditions

In the fixed blade simulations, the flow inlet, upstream of the blade, is set as a velocity inlet with a velocity magnitude of 69 m/s, which corresponds to a Mach number of 0.2. A zero-pressure gradient flow is obtained by using a pressure outlet as a boundary condition for the outlet. The plane of the domain in contact with the root of the blade is set as a symmetry plane and the rest of the boundaries are set as a free stream.

In the rotating blade simulations, the flow inlet is set as a velocity inlet. A

pressure outlet is set as the boundary condition for the outlet. The remaining four boundaries were set as free stream. At all boundaries, the velocity was set as 0 m/s. As a result of this, any movement in the flow simulations is solely caused by the rotation of the blade and the hub.

#### D. Numerical Methods

The simulations were performed using CD-adapco's CFD package, Star-CCM+<sup>39</sup>. The implicit unsteady model was used with the first-order temporal discretization. The flow equation model selected was coupled flow. A second order discretization scheme was used with implicit integration using the algebraic multigrid (AMG) linear solver for all flow variables. The AMG solver employed a Gauss-Seidel relaxation scheme with a bi-conjugate gradient stabilized acceleration method. A hybrid Gauss-Least Squares Quality (LSQ) method with the Venkatakrishnan limiter was used for gradients. The second order convection scheme with the AMG linear solver was applied to the turbulence model equations. A Gauss-Seidel relaxation scheme was also used for the turbulent variables without the acceleration method.

### IV. Results

#### A. Fixed Blade Simulations

The purpose of conducting the fixed-wing setting simulations was two-fold: i) to identify the mesh parameters necessary for resolving the tip vortex in simulations and ii) to analyze the effect of the blade shape on the size and intensity of the tip vortex.

It was found that to resolve the tip vortex, volumetric-controlled areas should be incorporated into the mesh. Figure 4a shows how the vortex structure looks like without the use of volumetric controls. The vortex shape resembles the cell element shape instead of being circular. By implementing two volumetric controls as described in the previous section, this issue was addressed as shown in Fig. 4b.

The mesh sensitivity study was conducted at the angle of attack of 10 degrees to determine the target element sizes in all regions of the mesh. To determine a number of mesh elements needed to obtain a mesh independent solution, the changes in the lift and drag coefficients  $C_L$  and  $C_D$  were monitored. It was found that these changes became minor when the number of mesh cells was increased from 2.2 to 3 million (Fig. 5). The difference in the values of  $C_L$  between the two finest meshes is of 0.2%. Similarly, the difference in the  $C_D$  values is about 0.5%.

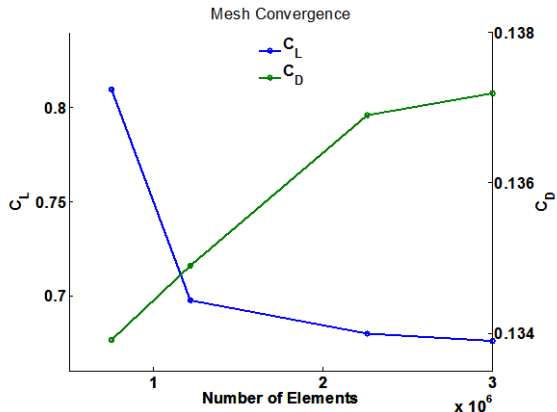


Figure 5. Mesh convergence results for  $C_L$  and  $C_D$ .

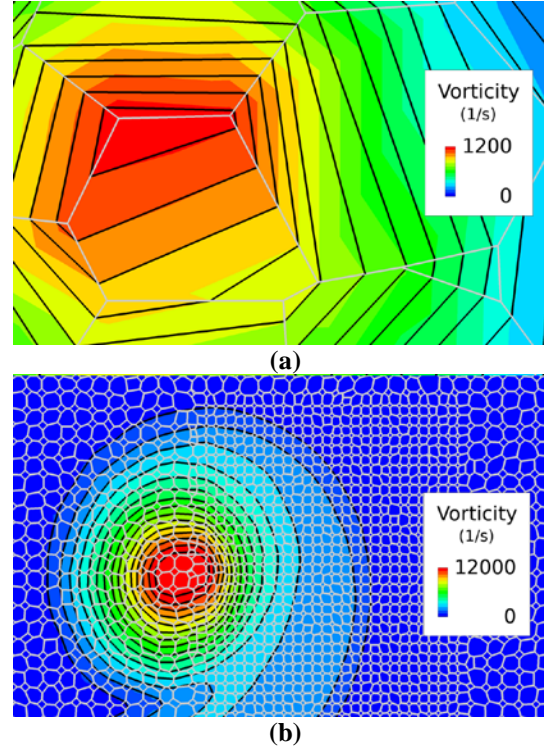


Figure 4. Vorticity magnitude contours outside (a) and inside (b) of volumetric controls.

Based on these results, the mesh with two volume controls that contains 2.2 million cells was chosen for analyzing the effect of the blade shape on the size and intensity of the tip vortex.

The effect of the blade shape was analyzed at three angles of attack: 0, 5, and 10 degrees. In the current paper, results are only presented for the 10-degree angle of attack at the chord-based Reynolds number of  $5.7 \times 10^4$ .

Two turbulence models were used in simulations: Menter's Shear Stress Transport (SST) version of the  $k-\omega$  model<sup>33</sup> and the Spalart-Allmaras (SA) model<sup>34</sup>. Differences in the results produced with the two models for the fixed blade setting were found to be negligible. Therefore, results presented are those obtained with the SST turbulence model.

In Figure 6, the vorticity contours at distances of 1, 3, and 7 chord lengths downstream of the blade are compared for the bio-inspired (left) and rectangular (right) blades. As demonstrated in the figure, the vorticity magnitude decreases more rapidly behind the bio-inspired blade. Similar observations can be made for the turbulence kinetic energy  $k$  (Fig. 7). The rectangular blade generates a vortex with higher values of  $k$  than the bio-inspired blade does. The area of higher turbulent kinetic energy level behind the blade tip is larger for the rectangular blade. The midrange values of  $k$  for the bio-inspired wing are projected between one and two chord lengths (13-26 mm) behind the blade, whereas the rectangular blade has midrange values that extend twice as far (26-52 mm). The decrease in vorticity and  $k$  shown in Figs. 6 and 7 confirms that using the bio-inspired blade reduces the strength and size of the tip vortex.

Once the location and size of the vortex core for a given downstream distance was determined, the profiles of turbulent kinetic energy, velocity deficit,  $U_D$ , and tangential velocity,  $u_\theta$ , were used to compare the near-wake flow structure behind the bio-inspired blade and the rectangular one. In Figure 8, these profiles are shown at the distance of one chord length downstream of each blade.

The level of turbulent kinetic energy is higher behind the rectangular blade across most of the vortex (Fig. 8a). The maximum difference between the  $k$ -profiles for rectangular and bio-inspired blades is about 35%. The difference in the maximum value of the axial velocity deficit defined as

$$U_D = -\frac{w-U_\infty}{U_\infty} \quad (2)$$

is about 15% less for the bio-inspired blade (Fig. 8b). The magnitude of the tangential velocity in the tip vortex behind the rectangular blade is greater over most of the profile (Fig. 8c), which translates to a stronger vortex. A decrease in the tangential velocity for the tip vortex behind the bio-inspired blade should alleviate noise and vibratory airloads on an aircraft<sup>35</sup>.

For comparison, a profile for the Burger's vortex is also shown in Fig. 8c. A two-dimensional Burgers' vortex<sup>36</sup> corresponds to a laminar vortex produced by radial inflow and axial outflow and can be obtained from the following equation<sup>37</sup>:

$$\frac{u_\theta}{u_{\theta \max}} = \frac{1.398}{r/r_c} \left\{ 1 - \exp \left[ -1.256 \left( \frac{r}{r_c} \right)^2 \right] \right\}.$$

There is some disagreement between the three profiles shown in Fig. 8c at the negative values of  $r/r_c$ , which can be attributed to the flow turbulence and to the flow-blocking effect that the blade geometry has on the downstream flow field. However, the overall trend is satisfied by both tip vortices. The shape and values seen in Fig. 8 match those found in Refs. 3, 15, 38, and 39, confirming the validity of the simulation results.

In Figure 8, the vortex core radius  $r_c$  is used to normalize the radial distance from the vortex core center. The

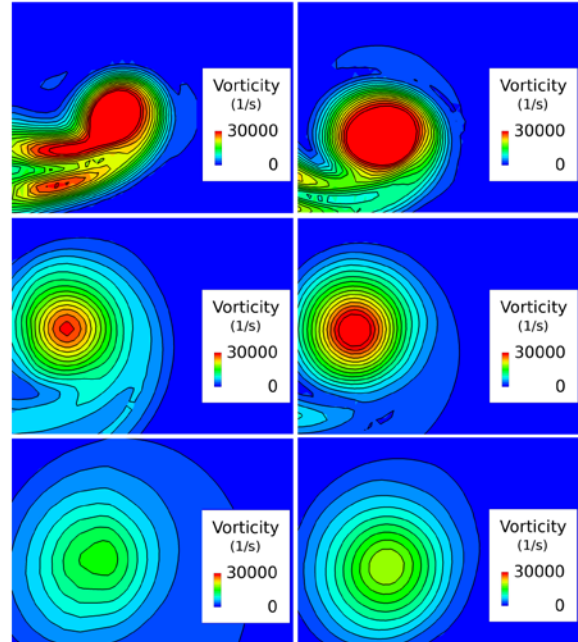


**Figure 6. Vorticity contours for bio-inspired (left) and rectangular (right) blades at mid-chord distances of 1c (top), 3c (middle), and 7c (bottom).**

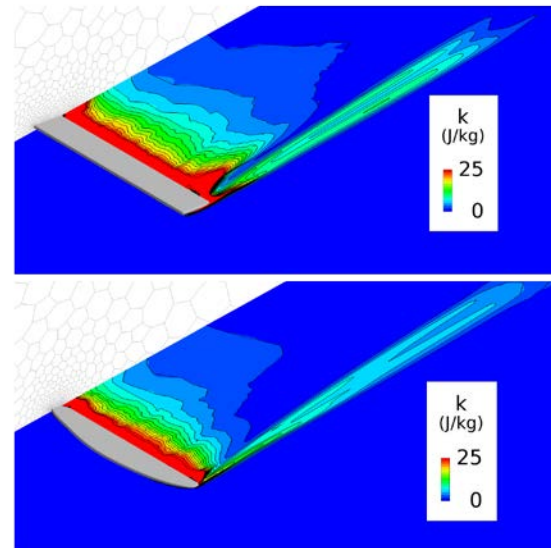


**Figure 7. Turbulent kinetic energy contours for the rectangular (top) and bio-inspired (bottom) blades.**

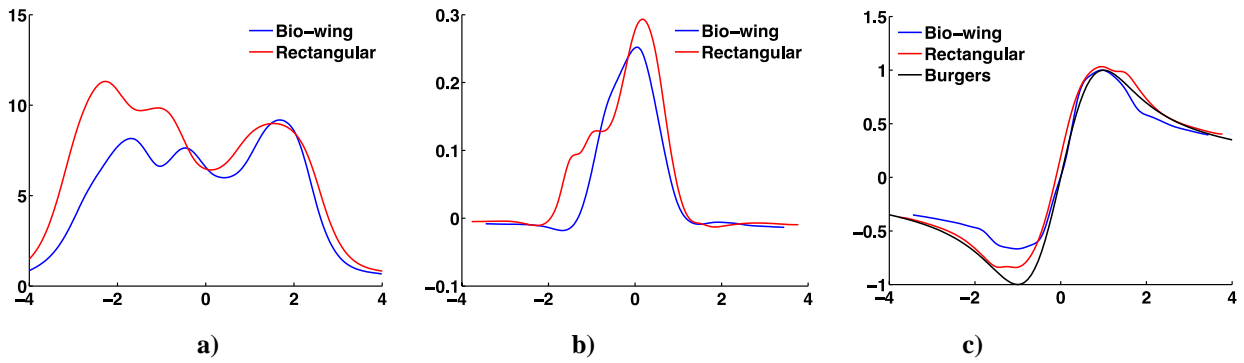


**Figure 8. Flow parameters at the vortex core: a) turbulent kinetic energy, b) axial velocity deficit, c) tangential velocity.**

vortex core radius is defined as a half of the distance between the peaks of the tangential velocity profile shown in Fig. 8c. The vortex core radius is about  $1.25 \times 10^{-3}$  m at the location of data collection for both blades.

### B. Rotating Blade

A mesh convergence study was conducted for the rotating blade simulations. Four grid configurations ranging from 611,000 elements to 3,179,000 elements were generated for this purpose. The lift coefficient,  $C_L$ , was monitored for the rectangular blade at the simulation time 5 s. Figure 9 shows that the lift coefficient changed by 0.3% when a number of cells was increased from 2 to 3 million. Based on these results, the 2 million cell mesh was chosen for the following simulations.

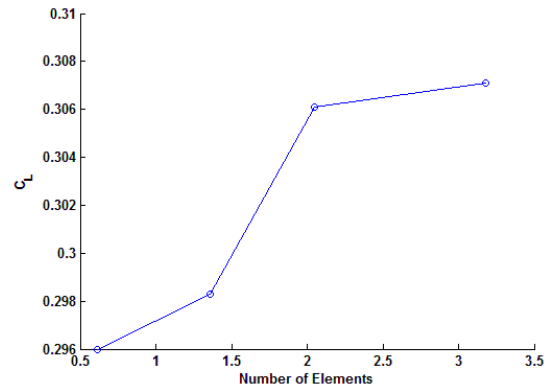


**Figure 9. The Mesh convergence results for  $C_L$  in the rotating plate.**

A time-step sensitivity study was also conducted to select the suitable time step interval for the rotating blade simulations. Two time steps were used, 0.01s and 0.001s. Total time span was 5 s. The lift coefficients were monitored for each blade and it was found that the time step interval had a very small effect on the lift coefficient ( $C_L$  values changed by less than 0.01%). However, the wake shape differed greatly depending on the time step. The smallest time step 0.001s was chosen for the following simulations as it yielded lower residuals.

The results shown in Figs. 10-12 correspond to the blades at the 10 degree angle of attack, rotating at 6 rps. The simulations were conducted over a 10 s time span. Menter's Shear Stress Transport (SST) version of the  $k-\omega$  model<sup>33</sup> was used with the curvature correction enabled. The curvature correction allows for more accurate simulation of swirling flows, such as the flow in the wake of a rotating blade.

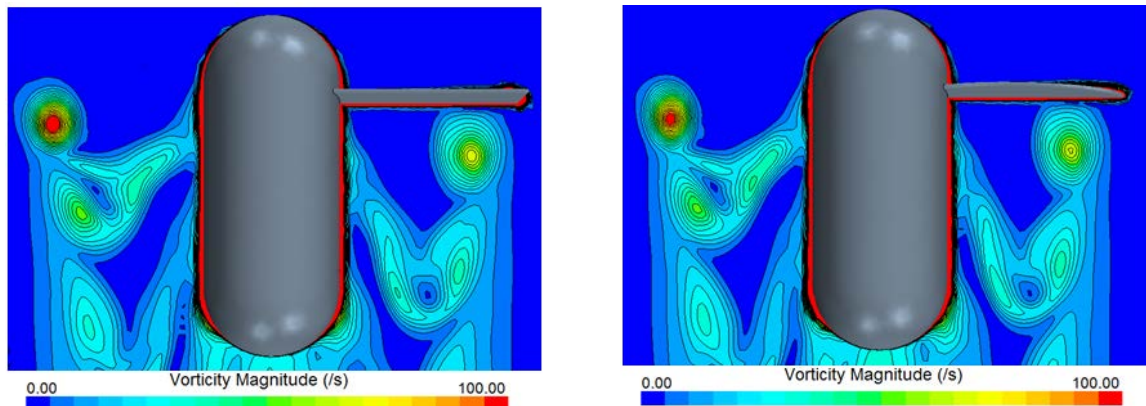


**Figure 10. Vorticity magnitude contours for the rectangular (a) and bio-inspired (a) blades.**

Vorticity contours were compared for both blades at planes located at  $y = 0$ . Figures 10 and 11 show the contours for both the rectangular and the bio-inspired blades. In Fig. 10, the vortex on the left side is the one shed most recently from the blade. The vortex close-up is given in Fig. 11. Qualitatively, it appears that the areas of high intensity are smaller for the vortex generated by the bio-inspired blade than that of shed from the rectangular blade. The vorticity magnitude decreases for both blades as the vortex travels downstream from a blade.

The turbulent kinetic energy contours are shown in Fig. 12. The contours correspond to a distance of 10.25 chords from the inlet, which is the blade location. The rectangular blade has higher values of  $k$  that are distributed over a greater area than in the bio-inspired blade flow. The mid-range  $k$  values extend longer into the wake on the rectangular blade than they do in the wake behind the bio-inspired blade. This indicates that the vortex behind the bio-inspired blade is smaller and weaker than in the rectangular blade wake.

In Figure 13, the profiles of turbulent kinetic energy, velocity deficit, and tangential velocity are shown for the two blades at the same location as the vortices in Fig. 6. At this location, the vortices behind the both blades have the vortex core radius of 0.08 m. The vortex behind the bio-inspired blade has lower values of  $k$  across most of the vortex (Fig. 13a). The maximum decrease in the  $k$ -value is 23% (0.0191 J/kg) in the vortex behind the bio-inspired blade to compare with that is observed in the vortex behind the rectangular blade. The peak of the axial velocity deficit in the vortex behind the bio-inspired blade is 52% less than that of in the vortex generated by the rectangular blade (Fig. 13b). In a case of rotating blades, the velocity deficit is defined similar to (2), except that the tip velocity is used in place of the freestream velocity. The tangential velocity profiles of the two blades are close in values (Fig. 13c). Overall, the profiles of turbulent kinetic energy, velocity deficit, and tangential velocity confirm that the vortex generated behind rotating bio-inspired blade is smaller and weaker than the one behind the rotating rectangular blade.

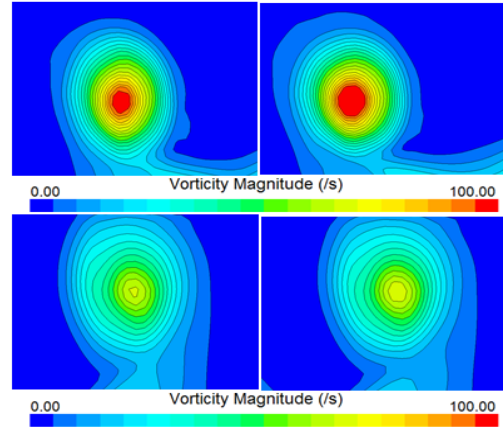


**Figure 11. The vorticity contour close-ups for the bio-inspired (left) and rectangular (right) blades at  $y = 0$ .**

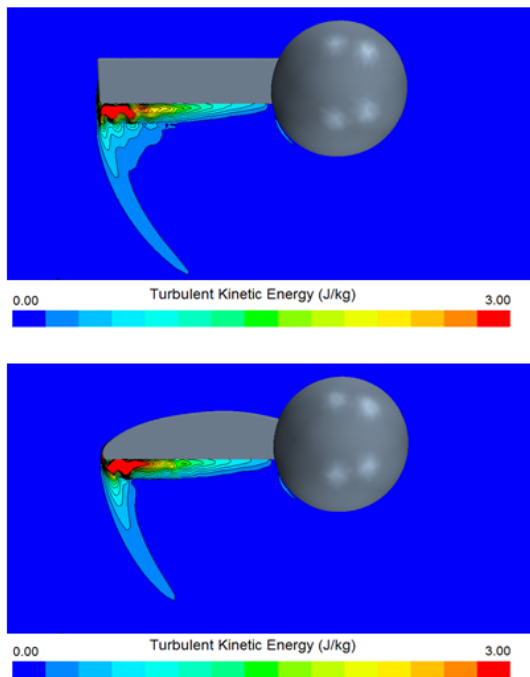


**Figure 12. Turbulent kinetic energy contours for the rectangular (top) and bio-inspired (bottom) blades.**

## V. Conclusion

In the current study, the analysis of the insect orders with the purpose of determining an insect whose flight characteristics are close to the design parameters of a small rotorcraft was conducted. Cicadas were determined as the most favorable specie to study. Computational analysis of a flow structure around and behind fixed and rotating blades with the shape of a cicada wing was performed to identify potential benefits of using such a wing as a prototype for aerodynamic applications. Simulations were conducted at different angles of attack. Particular focus was given to the tip vortex generated by the blades. Contours of vorticity and turbulent kinetic energy along with the profiles of turbulent kinetic energy, axial velocity deficit, and tangential velocity in the near-wake of fixed and rotating bio-inspired blades were compared with those corresponding to fixed and rotating rectangular blades with the matching span length and surface area. Simulation results demonstrated the advantages of the bio-inspired blade. That is, the vortex size and strength is reduced aft of the blade tip.

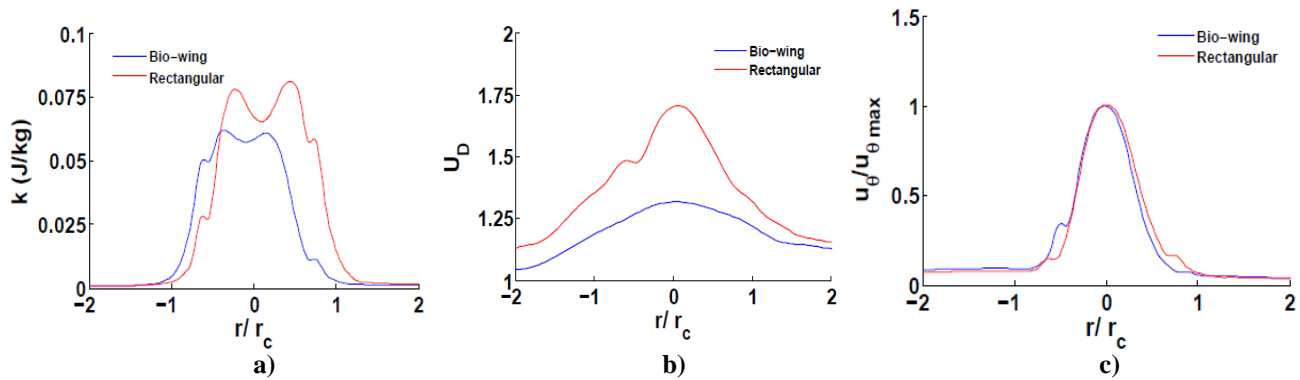


**Figure 13. Flow parameters at the vortex core behind rotating blades: a) turbulent kinetic energy, b) axial velocity deficit, c) tangential velocity.**

### Acknowledgments

Simulations were conducted using high-performance facilities of the Center for Advanced Research Computing, University of New Mexico. A part of work was supported by NASA under award NNX12AJ61A. The New Mexico Space Grant Consortium and the Office of Graduate Studies at The University of New Mexico supported Sebastian Gomez's research. The authors also acknowledge support from CD-adapco, Intelligent Light, and Dassault Systèmes for providing Star-CCM+, FieldView, and SolidWorks for academic purposes.

### References

- <sup>1</sup>Shyy, W., and Liu, H., "Flapping Wings and Aerodynamic Lift: The Role of Leading-Edge Vortices," *AIAA Journal*, Vol. 45, No. 12, 1996, pp. 2817-2819.
- <sup>2</sup>Green, S. I., *Fluid Vortices: Fluid Mechanics and Its Applications*, Vol. 1, Kluwer Academic Publishers, Netherlands, 1995, Chap. 10.
- <sup>3</sup>Wells, J., "Effects of Turbulence Modeling on RANS Simulations of Tip Vortices," M.S. Thesis, Engineering Mechanics Dept., Virginia Polytechnic Institute and State University, Blacksburg, VA, 2009.
- <sup>4</sup>Viieru, D., Albertani, R., Shyy, W., and Ifju, P., "Effect of Tip Vortex on Wing Aerodynamics of Micro Air Vehicles," *Journal of Aircraft*, Vol. 42, No. 6, November – December 2005, pp. 1530-1536.
- <sup>5</sup>Ning, S. A., and Kroo, I., "Multidisciplinary Considerations in the Design of Wings and Wing Tip Devices," *Journal of Aircraft*, Vol. 47, No. 2, March – April 2010, pp. 534-543.
- <sup>6</sup>Kroo, I., "Drag Due to Lift: Concepts for Prediction and Reduction," *Ann. Rev. Fluid Mech.*, Vol. 33, 2001, pp. 587-617, URL: <http://www.annualreviews.org/doi/pdf/10.1146/annurev.fluid.33.1.587> [cited 15 August 2013].
- <sup>7</sup>Widnall, S., "Helicopter Noise due to Blade-Vortex Interaction," *Journal of the Acoustical Society of America*, Vol. 50, No. 1, Part 2, July 1971, pp. 354-366.
- <sup>8</sup>Finch, R., Coronado, CA, U.S. Patent Application for a "Vortex Reducing Wing Tip," Patent No. 4,108,403, filed 22 Aug. 1978.
- <sup>9</sup>McCarthy, P. T., Buffalo, NY, U.S. Patent Application for a "Tip Vortex Generation Technology for Creating a Lift Enhancing and Drag Reducing Upwash Effect," Patent No. 5,634,613, filed 3 Jun. 1997.
- <sup>10</sup>Vogt, R., Hamburg, Germany, U.S. Patent Application for a "Twisted Wing Tip Fin for Airplanes," Patent No. 2,576,981, filed 4 Dec. 1951.
- <sup>11</sup>Taylor, R. M., U.S. Navy, Washington, D.C., U.S. Patent Application for an "Aerodynamic Surface Tip Vortex Attenuation System," Patent No. 5,158,251, filed 27 Oct. 1992.
- <sup>12</sup>Ngo, H. T., McDonnell Douglas Helicopter Co., Mesa, AZ, U.S. Patent Application for a "Tip Vortex Reduction System," Patent No. 5,791,875, filed 11 Aug. 1998.
- <sup>13</sup>Hassan, A. A., Straub, F. K., Domzalski, D. B., Kennedy, D. K., McDonnell Douglas Helicopter Co., Mesa, AZ, U.S. Patent Application for a "Active Blowing System for Rotorcraft Vortex Interaction Noise Reduction," Patent No. 5,813,625, filed 29 Sep. 1998.
- <sup>14</sup>Charles, B. D., Hassan, A. A., Tadghighi, H., JanakiRam, R. D., Sankar, L. N., McDonnell Douglas Helicopter Co., Mesa, AZ, U.S. Patent Application for a "Blade Vortex Interaction Noise Reduction Techniques for a Rotorcraft," Patent No. 5,588,800, filed 31 Dec. 1996.
- <sup>15</sup>Pierson, K., "Vorticity Confinement Technique for Preservation of Tip Vortex of Rotating Blade," *31<sup>st</sup> AIAA Applied Aerodynamics Conference*, AIAA 2013-2420, San Diego, CA, 2013.
- <sup>16</sup>Tucker, V. A., "Gliding Birds: Reduction of Induced Drag by Wing Tip Slots Between the Primary Feathers," *Journal of Experimental Biology*, Vol. 180, 1993, pp. 285-310.
- <sup>17</sup>Bushnell, D. M., "Drag Reduction in Nature," *Annu. Rev. Fluid Mech.*, Vol. 23, 1991, pp. 65-79, URL: <http://www.annualreviews.org/doi/pdf/10.1146/annurev.fl.23.010191.000433> [cited 19 August 2013].

- <sup>18</sup>Dickinson, M. H., "Wing Rotation and the Aerodynamic Basis of Insect Flight," *Science*, Vol. 284, 1999, pp. 1954-1960.
- <sup>19</sup>Ellington, C. P., "The Novel Aerodynamics of Insect Flight: Applications to Micro-Air Vehicles," *Journal of Experimental Biology*, Vol. 202, 1999, pp. 3439-3448.
- <sup>20</sup>Wang, Z. J., "Two Dimensional Mechanism for Insect Hovering," *Physical Review Letters by the American Physical Society*, Vol. 85, No. 10, 2000, pp. 2216-2218.
- <sup>21</sup>Rees, C. J. C., "Aerodynamic Properties of an Insect Wing Section and a Smooth Aerofoil Compared," *Nature*, Vol. 258, November, 1975. pp. 141-142.
- <sup>22</sup>Young, J., Walker, S. M., Bomphrey, R. J., Taylor, G. K., and Thomas, A. L. R., "Deformation Enhance Aerodynamic Function and Flight Efficiency," *Science*, Vol. 325, 2009. pp. 1549-1552.
- <sup>23</sup>Vargas, A., and Mittal, R., "Aerodynamic Performance of Biological Airfoils," *AIAA 2<sup>nd</sup> Flow Conference*, AIAA 2004-2319, Portland, OR, 2004.
- <sup>24</sup>Kim, W., Ko, J. H., Park, H. C., and Byun D., "Aerodynamic Performance of Biological Airfoils," *Journal of Theoretical Biology*, Vol. 260, 2009, pp. 523-530.
- <sup>25</sup>Vargas, A., Mittal, R., and Dong, H., "A Computational Study of the Aerodynamic Performance of a Dragonfly Wing Section in Gliding Flight," *Bioinspiration & Biomimetics*, Vol. 3, 2008, 026004.
- <sup>26</sup>Tamai, M., Wang, Z., Rajagopalan, G., Hu, H., and He, G., "Aerodynamic Performance of a Corrugated Dragonfly Airfoil Compared with Smooth Airfoils at Low Reynolds Numbers," *45<sup>th</sup> AIAA Aerospace Sciences Meeting and Exhibit*, AIAA 2007-0483, Reno, NV, 2007.
- <sup>27</sup>Ringuette, M., Milano, M., and Gharib, M., "Role of the Tip Vortex in the Force Generation of Low-aspect-ratio Normal Flat Plates," *Journal of Fluid Mechanics*, Vol. 581, 2007, pp. 453-468.
- <sup>28</sup>Evans, J. D., and Gundersen-Rindal, D., "Beenomes to Bombyx: Future Directions in Applied Insect Genomics," *Genome Biology*, Vol. 4, No. 3, 2003, Article 107.
- <sup>29</sup>Handy, C., "Nature-inspired Rotorcraft Blade Design," M.S. Project Report, Mechanical Engineering Dept., University of New Mexico, Albuquerque, NM, 2012.
- <sup>30</sup>Deakin M. A. B., "Formulae for Insect Wing beat Frequency," *Journal of Insect Science*, Vol. 10, 2010, Article 96.
- <sup>31</sup>Byrne, D. N., "Relationship Between Wing Loading, Wing beat Frequency, and Body Mass In Homopterous Insects," *Journal of Experimental Biology*, Vol. 135, 1988, pp. 9-23.
- <sup>32</sup>Dudley, R., *The Biomechanics of Insect Flight: Form, Function, Evolution*, 2<sup>nd</sup> Edition, Princeton University Press, New Jersey, 2000, Chap. 3.
- <sup>33</sup>Dacles-Mariani, J., Kwak, D., and Zilliac, G., "On Numerical Errors and Turbulence Modeling in Tip Vortex Flow Prediction," *Journal for Numerical Methods in Fluids*, Vol. 30, 1999, pp. 65-82.
- <sup>34</sup>Burgers, J. M., "A Mathematical Model Illustrating the Theory of Turbulence," *Advances in Applied Mechanics*, Vol. 1, Academic Press, New York, 1948, pp. 171-199.
- <sup>35</sup>Sousa, J. M. M., Pereira, J. C. F., "Rollup Region of a Turbulent Trailing Vortex Issued from a Blade with Flow Separation," *Experimental Thermal and Fluid Science*, Vol. 20, 2000, pp. 150-161.
- <sup>36</sup>Revell, A., Iaccarino, G., and Wu, X., "Advanced RANS Modeling of Wingtip Vortex Flows," *Proceedings of the Summer Program 2006*, Center for Turbulence Research, Stanford, CA, 2006.
- <sup>37</sup>Martin, P. B., Leishman, J. G., "Trailing Vortex Measurements in the Wake of a Hovering Rotor Blade with Various Tip Shapes," *58<sup>th</sup> Annual Forum of the AHS International*, Montreal, Canada, 2002.